THE JOURNAL OF PHYSICAL CHEMISTRY C

Article

pubs.acs.org/JPCC

Prediction of *n*-Alkane Adsorption on Activated Carbon Using the SAFT−FMT−DFT Approach

Lucas A. Mitchell, Bryan J. Schindler, Gaurav Das, Maria Carolina dos Ramos, Clare McCabe, Peter T. Cummings, and M. Douglas LeVan*

Department of Chemical and Biomolecular Engineering, Vanderbilt University, Nashville, Tennessee 37235, United States

Supporting Information

ABSTRACT: The SAFT−FMT−DFT approach to adsorption equilibrium combines elements of the statistical associating fluid theory (SAFT), fundamental measure theory (FMT), and classical density functional theory (DFT) to create a framework to model fluids described as chain molecules in the presence of external fields. In this paper, the SAFT−FMT−DFT approach is used to calculate single pore isotherms to develop a pore size distribution for BPL activated carbon, described by the 10−4−3 fluid-wall potential, based on nitrogen adsorption at 77 K. The nitrogen pore isotherms show a progression of monolayer transitions, pore filling, and pore condensation. The pore size distribution is used to predict excess adsorption isotherms for methane, ethane, *n*-butane, *n*-pentane, and *n*-hexane adsorbed on the carbon at 298.15 and 348.15 K. Parameters for interaction of the molecules with the solid are obtained using experimental data for adsorption of each alkane on the planar wall of a nonporous graphitized carbon. The predicted excess *n*-alkane isotherms agree well with experimental isotherms.

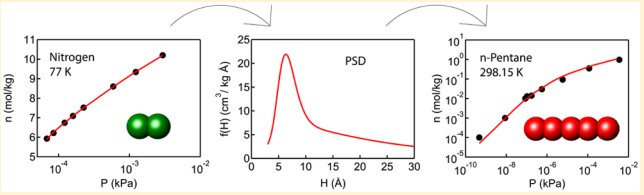

1. INTRODUCTION

In a recent paper,[1] we introduced a new theory, which we referred to as a SAFT−FMT−DFT approach, to describe the adsorption of chain molecules in slit shaped pores. The theory combines elements of the statistical associating fluid theory (SAFT), fundamental measure theory (FMT), and classical density functional theory (DFT) to create a framework to model fluids in the presence of external fields. Theoretical predictions were shown to agree well with several Monte Carlo simulations of adsorption in the literature. The present paper uses the SAFT−FMT−DFT approach to predict the adsorption of *n*-alkanes in activated carbon from fundamental parameters and properties obtained independently and compares the predictions with experimental data.

Many classical DFTs have been proposed to determine equilibrium properties for an inhomogeneous fluid by finding a density distribution that minimizes the Helmholtz free energy. Of relevance to this paper are those that have been developed to characterize adsorbent materials and predict adsorption equilibrium. The most common goal of these DFTs is to determine the pore size distribution of an adsorbent, which is performed by first calculating fluid densities for different pore sizes and then developing a pore size distribution that sums the individual pore isotherms to match an experimental adsorption isotherm, usually nitrogen at 77 K.[2−6] DFTs have also been used to model adsorption isotherms of various fluids on activated carbons and other materials at and above cryogenic temperatures by calculating individual pore isotherms and summing them at selected pressures according to a known pore size distribution.[7−14]

SAFT[15] is a molecular based equation of state that has been developed using the thermodynamic perturbation theory of Wertheim[16−19] to describe properties of chain molecules. The monomer segments of the chain interact via dispersion and association sites that mimic molecular association interactions, such as hydrogen bonding. Within SAFT, the Helmholtz free energy is calculated by summing contributions describing monomer−monomer interactions, chain connectivity, and intermolecular association. Many versions of SAFT have been proposed, and these have been thoroughly reviewed by McCabe and Galindo,[20] who also discuss the many systems to which they have been applied. Furthermore, our previous paper[1] provides a lengthy and detailed discussion of the various implementations of SAFT that are related to this work. The SAFT−FMT−DFT approach uses a version of SAFT-VR,[21] the statistical associating fluid theory for potentials of variable range, which maintains a close formal link with the molecular model. In SAFT-VR, the monomer−monomer interactions within a chain molecule are treated using a square-well potential.

FMT[22,23] is a rigorous approach for the treatment of density distributions in inhomogeneous hard sphere and hard cylinder fluids. In the SAFT−FMT−DFT approach, FMT is used to describe the hard-sphere and hard-sphere chain interactions and allows SAFT-VR to describe the attractive potential using perturbation terms rather than a mean-field approximation,

Received: October 19, 2014
Revised: December 16, 2014
Published: December 18, 2014

DOI: 10.1021/jp510515m
J. Phys. Chem. C 2015, 119, 1457−1463

which is common to many SAFT-based DFT approaches. Thus, the use of FMT extends SAFT-VR strictly and precisely from a theory for a homogeneous fluid in the bulk to a theory for an inhomogeneous fluid near boundaries such as pore walls.

SAFT has previously been incorporated into DFTs to model complex fluids, including mixtures of chain molecules, as discussed in our earlier paper.[1] Recently, Shen et al.[24,25] have incorporated the perturbed-chain statistical associating fluid theory (PC-SAFT) with FMT into a DFT using the chain free energy functional of Tripathi and Chapman,[26] which involves the use of bulk fluid properties obtained from a mean-field level SAFT but allows the use of a noninterger number of monomer units in the model chain. They used a weighted density approximation to represent dispersive attraction contributions to free energy, and parameters were regressed from data for methane and carbon dioxide adsorbed on an activated carbon using a single pore width or a pore size distribution, Lennard-Jones well depths, and independent surface areas to model the components in a binary mixture. Also, Malheiro et al.[27] coupled SAFT-VR and FMT in a DFT that did not include the chain and associating contributions of SAFT-VR and used instead a mean-field approximation; they obtained good agreement between theoretical predictions and experimental results for methane adsorbed in a carbon molecular sieve.

In this paper, we use our SAFT−FMT−DFT approach[1] to calculate density profiles for nitrogen and several *n*-alkanes in carbon parallel slit pores. The dispersive attractive contribution to the free energy in SAFT is treated using first- and second-order perturbation terms rather than a mean-field approximation. For all adsorbates, we determine fluid−fluid parameters by fitting model results to pure component vapor pressure and vapor−liquid density data. The slit-shaped pores of the activated carbon are described using the popular 10−4−3 potential.[28] The well depth of the potential is determined for all adsorbates by fitting predictions of the model to experimental data for adsorption on the planar wall of a nonporous graphitized carbon. An experimental isotherm[29] for nitrogen adsorption at 77 K is used with the calculated single pore nitrogen isotherms to determine a pore size distribution for BPL activated carbon. This pore size distribution is used with the single pore isotherms for methane, ethane, *n*-butane, *n*-pentane, and *n*-hexane at 298.15 and 348.15 K to predict excess isotherms for adsorption on the carbon, and these are compared with experimental data[30−32] for adsorption of each alkane at the two temperatures. Notably, all parameters in the theory for adsorption of the alkanes on the activated carbon are evaluated independently and a priori, either from vapor−liquid data, adsorption on nonporous walls, or nitrogen adsorption. The treatment of data for adsorption of the alkanes on the activated carbon therefore involves no additional fitted parameters and is purely predictive.

2. THEORY

Density functional theory is used to calculate the density profile that minimizes the grand potential function $\Omega[\rho_m(\mathbf{R})]$, where $\rho_m(\mathbf{R})$ is the density profile of a chain molecule as a function of segment position $\mathbf{R} \equiv (\mathbf{r}_1, \mathbf{r}_2, ..., \mathbf{r}_m)$ and m is the number of segments in the chain. This is done by setting the functional derivative with respect to the density equal to zero. The grand potential is calculated by

$$\Omega[\rho_m(\mathbf{R})] = F[\rho_m(\mathbf{R})] + \int \rho_m(\mathbf{R})[V_{ext}(\mathbf{R}) - \mu]\, d\mathbf{R} \quad (1)$$

where $F[\rho_m(\mathbf{R})]$ is the Helmholtz free energy, μ is the chemical potential for the chain molecule, and $V_{ext}(\mathbf{R})$ is the external potential. To introduce a version of SAFT, we write the Helmholtz free energy as

$$F = F_{id} + F_{hs} + F_1 + F_2 + F_{chain} \quad (2)$$

where the terms correspond to the ideal, hard sphere, first-order attractive, second-order attractive, and chain contributions, respectively.

The general development of the SAFT−FMT−DFT approach has been published recently[1] and will not be reproduced here. We describe below only specific details associated with the application of the theory to the systems considered in this work.

The hard sphere repulsive term is calculated using the improved FMT of Hansen-Goos and Roth[33] for a Carnahan−Starling−Boublík fluid. The chain term was developed by Yu and Wu[34] for a hard sphere chain. The attractive terms use a perturbation analysis expanded out to second order, rather than the commonly adopted mean-field approximation.

The external potential of the carbon for the solid−fluid interaction is described by

$$V_{ext} = \phi_{sf}(z) \quad (3)$$

for a planar wall, where z is distance from the wall, and by

$$V_{ext} = \phi_{sf}(z) + \phi_{sf}(H - z) \quad (4)$$

for a slit pore of width H. $\phi_{sf}(z)$ is given by the 10−4−3 potential[28]

$$\phi_{sf}(z) = 2\pi\epsilon_{sf}\rho_s\sigma_{sf}^2\Delta\left[\frac{2}{5}\left(\frac{\sigma_{sf}}{z}\right)^{10} - \left(\frac{\sigma_{sf}}{z}\right)^4 - \frac{\sigma_{sf}^4}{3\Delta(z + 0.61\Delta)^3}\right] \quad (5)$$

where ϵ_{sf} and σ_{sf} are Lennard-Jones potential parameters, $\rho_s = 0.114$ Å^{-3} is the bulk density of carbon atoms in the walls, and $\Delta = 3.35$ Å is the carbon layer spacing in the multilayered walls.

Taking the functional derivative of eq 1 and rearranging results in the equation used to calculate the segment equilibrium density profile:[34]

$$\rho(z) = \frac{1}{\Lambda^3}\exp(\mu)\sum_{i=1}^{m}\exp\left[-\frac{\psi(z)}{kT}\right]G^i(z)G^{m+1-i}(z) \quad (6)$$

with

$$\psi(z) \equiv \frac{\delta F_{hs}}{\delta\rho(\mathbf{r})} + \frac{\delta F_1}{\delta\rho(\mathbf{r})} + \frac{\delta F_2}{\delta\rho(\mathbf{r})} + \frac{\delta F_{chain}}{\delta\rho(\mathbf{r})} + V_{ext} \quad (7)$$

and

$$G^i \equiv \int \exp\left[-\frac{\psi(z)}{kT}\right]\frac{\Theta(\sigma_{ff} - |z - z'|)}{2\sigma_{ff}}G^{i-1}\, dz' \quad (8)$$

where $\rho(\mathbf{r})$ is the monomer density, Λ is the de Broglie wavelength, Θ is the Heaviside step function, σ_{ff} is the hard sphere diameter, and $G^1(z) = 1$. The solution method involves iterating on the segment density. Because of the summation in eq 6, the value of the parameter m is restricted to integer values.

The equilibrium value of the density, given by eq 6, is used to determine the excess density in the pore using

DOI: 10.1021/jp510515m
J. Phys. Chem. C 2015, 119, 1457−1463

$$\rho_{ex}(H, P) = \frac{1}{H}\int_0^H \left[\frac{\rho(z)}{m} - \rho_b\right] dz \quad (9)$$

where ρ_b is the bulk density. As indicated, with temperature specified, this excess density will be a function of pore width H and pressure P.

The pore size distribution is determined by comparing experimental isotherm data with the calculated isotherms, which are obtained by integrating the excess densities in pores over the range of pore widths and pressures using the adsorption integral equation

$$n(P) = \int_0^\infty \rho_{ex}(H, P) f(H)\, dH \quad (10)$$

where $f(H)$ is the pore size distribution. The model used for the pore size distribution is a log-normal distribution

$$f(H) = \frac{1}{\sqrt{2\pi}H}\sum_{i=1}^{M}\frac{\alpha_i}{\gamma_i}\exp\left[-\frac{(\ln H - \beta_i)^2}{2\gamma_i^2}\right] \quad (11)$$

where M is the number of modes and α_i, β_i, and γ_i are parameters.

3. RESULTS AND DISCUSSION

Several steps are required for the pure prediction of the alkane isotherms on the activated carbon. First, fluid−fluid parameters must be established for the SAFT-VR equation of state. Second, solid−fluid parameters must be obtained for the interaction of molecules with an ideal adsorbent surface. Third, a pore size distribution must be obtained for the activated carbon. Then, the alkane isotherms can be predicted. Each of these steps involves comparisons with experimental data as described below. The determination of all parameters in this work involved the use of least-squares criteria. All data on BPL activated carbon analyzed in this work, for nitrogen and all alkanes, were measured on samples from a single container of the adsorbent (Calgon Carbon Corp., Lot No. 4814-J).

Fluid−Fluid Parameters. To describe the fluid−fluid interactions with the SAFT-VR approach, the specification of four fluid−fluid parameters is required for each molecule. One of these, m, the number of segments in a molecule, was prescribed to be an integer value to allow the use of eq 6. We used m = 2 for nitrogen and m equal to the number of carbon atoms for the alkanes. The remaining fluid−fluid parameters σ_{ff}, ϵ_{ff}, and λ (the Lennard-Jones diameter, the Lennard-Jones well depth, and the range of the attractive interactions, respectively) were fit using vapor−liquid equilibrium data and a nonlinear regression method,[35,36] as detailed in the Supporting Information. The fluid−fluid parameters for nitrogen and all of the alkanes studied are given in Table 1.

Table 1. Model Parameters

		fluid−fluid			solid−fluid	
molecule	m	σ_{ff} (Å)	ϵ_{ff}/k (K)	λ	σ_{sf} (Å)	ϵ_{sf}/k (K)
nitrogen	2	2.657	40.28	1.832	3.018	42.98
methane	1	3.670	168.8	1.444	3.525	65.68
ethane	2	3.136	129.6	1.691	3.258	68.80
n-butane	4	2.821	70.50	2.034	3.100	74.09
n-pentane	5	2.791	57.08	2.163	3.086	74.63
n-hexane	6	2.740	50.00	2.253	3.060	75.56

Solid−Fluid Parameters. Two solid−fluid parameters are imbedded in the theory, σ_{sf} and ϵ_{sf}. Following Lastoskie et al.[2] and many others, the solid diameter σ_{sf} was calculated using the Lorentz−Berthelot mixing rule

$$\sigma_{sf} = \frac{\sigma_{ff} + \sigma_s}{2} \quad (12)$$

with the diameter of the carbon atom in the wall given by σ_s = 3.380 Å.

The solid−fluid potential ϵ_{sf} for nitrogen was determined by fitting the onset of the monolayer transition to experimental data for adsorption on a planar nonporous carbon wall. The data of Kruk et al.[37] were used for adsorption of nitrogen on Carbopack F, a commercially available graphitized carbon black with a BET surface area of 6.2 m^2/g. A wide pore of width H = 40 σ_{ff} was used in our SAFT-FMT-DFT model to simulate single nonporous walls, with adsorption on each wall being unaffected by the presence of the other wall.

The data of Avgul and Kiselev[38] for pure methane, ethane, *n*-butane, *n*-pentane, and *n*-hexane adsorbed on a graphite wall were used to determine ϵ_{sf} for the alkanes. The carbon used was a graphitized carbon black with a BET surface area of 12.2 m^2/g. As with nitrogen, a wide pore of width H = 40 σ_{ff} was used to simulate a nonporous surface.

The solid−fluid parameters are given in Table 1. Contributions of the $-CH_3$ and $-CH_2-$ groups to the σ and ϵ parameters for the fluid−fluid and solid−fluid interactions of the alkanes are provided in the Supporting Information.

Single Pore Isotherms for Nitrogen. Isotherms in pores of fixed width can now be predicted for all components with no additional parameters. As the pore size distribution of the activated carbon will be characterized using experimental data for nitrogen adsorption at 77 K, nitrogen isotherms must be predicted for pores of different sizes. These single pore isotherms, giving nitrogen density profiles across the pore, were obtained by solving eq 6 for many pore sizes at many pressures.

Figure 1 shows the density profiles for three different pore sizes, each at three different pressures: one before the monolayer transition, one after the monolayer transition, and one after pore condensation. Pores widths are 8.77, 10.63, and 11.03 Å, which correspond to 3.3, 4.0, and 4.15 σ_{ff}, with pore walls placed at z = 0 and z = H. Figures 1a−c show density profiles that are below the monolayer transition at a reduced pressure of 1.0×10^{-6}. It should be noted in these figures that the first peak does not occur at $z = \sigma_{ff}$ because the solid and the fluid segments have different sizes, with σ_{sf} = 3.018 Å and σ_{ff} = 2.657 Å. Thus, the first peak occurs at a value of z somewhat greater than σ_{ff}, near $z = \sigma_{sf} = 1.14\ \sigma_{ff}$. Figures 1d−f show density profiles that are above the monolayer transition at a reduced pressure of 1.0×10^{-5}. In Figure 1d, the peak has narrowed and the height has increased significantly, as a result of pore condensation. In contrast, at this pressure the larger pores shown in Figures 1e,f do not show pore condensation. Figures 1g−i show density profiles at a reduced pressure of 1.0×10^{-3}, with pore condensation in all three pores. In Figure 1g, the base of the peak has narrowed considerably and the height has increased. The increase is not as pronounced as for the larger pores, as condensation occurred in this small pore at a reduced pressure below 1.0×10^{-5}. In Figure 1h, the height of the peaks has increased significantly, and two smaller peaks have formed in the middle of the pore. These smaller peaks result from the larger peak interacting with its mirror image across the center line of the pore, with the left-center peak

DOI: 10.1021/jp510515m
J. Phys. Chem. C 2015, 119, 1457−1463

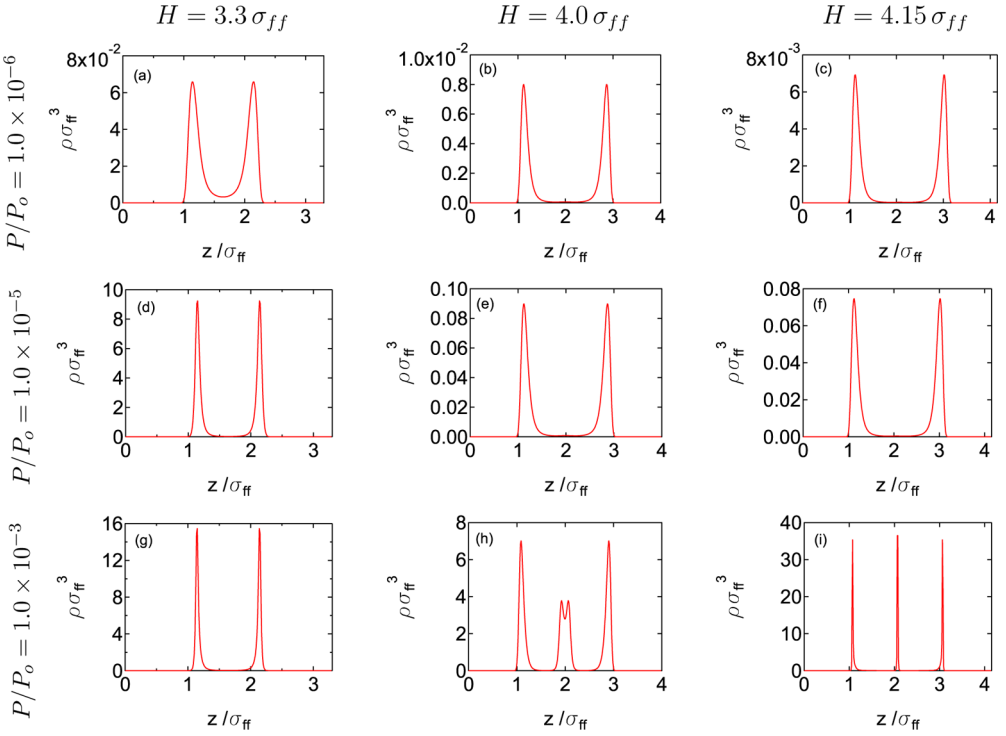

Figure 1. Nitrogen density profiles in pores of width 3.3, 4.0, and 4.15 σ_{ff} at 77 K for reduced pressures of 1.0×10^{-6}, 1.0×10^{-5}, and 1.0×10^{-3}. Note changes in scale of *y*-axis. P_0 = 1 atm.

associated with the right wall and the right-center peak associated with the left wall. As the pore expands, as shown in Figure 1i, the smaller peaks overlap, resulting in a much higher single peak.

Excess adsorption isotherms for different pore sizes were determined by calculating average excess densities, obtained by integrating the density profiles over the pore widths using eq 9, as a function of reduced pressure. Figure 2 shows the excess densities for nitrogen in pores of widths 2.55 σ_{ff}, 3 σ_{ff}, 3.5 σ_{ff}, 4 σ_{ff}, 5 σ_{ff}, and 6 σ_{ff}. The isotherm for the 3 σ_{ff} pore shows the monolayer transition occurring at a reduced pressure of 1×10^{-7}, with pore condensation at 4×10^{-7}. The 3.5 σ_{ff} pore has a less pronounced monolayer transition at a reduced pressure of 2×10^{-6}, with pore condensation at 5×10^{-6}. The 4 σ_{ff} pore isotherm has the monolayer transition at 1×10^{-5} and pore condensation at 3.7×10^{-5}. The isotherms for the 3.5 σ_{ff} and 4 σ_{ff} pores do cross near a reduced pressure of 3×10^{-4} because the size of the 3.5 σ_{ff} pore is far from an integer value of σ_{ff} and thus inconsistent with the formation of an additional layer of molecules. The 5 σ_{ff} pore shows the formation of the monolayer starting at a reduced pressure of 2×10^{-5}, multiple layers forming at 1×10^{-4}, and pore condensation occurring at a reduced pressure of 3.7×10^{-4}. For the 6 σ_{ff} pore, the monolayer forms at a reduced pressure of 2×10^{-5}, multiple layers of molecules occur at 1×10^{-4}, and pore condensation occurs at a reduced pressure of 2×10^{-3}. Thus, for adsorption of nitrogen at 77 K in pores up to 4 $\sigma_{ff} \approx 11$ Å in width, as the pore size increases, the monolayer transition shifts to higher pressures. For pores larger than 11 Å, the monolayer transition remains in the same place, but the formation of multiple layers and pore condensation move to higher pressures.

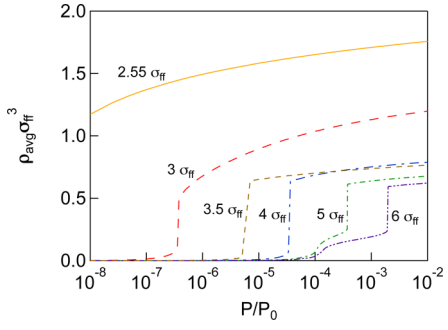

Figure 2. Single pore nitrogen excess isotherms at 77 K. P_0 = 1 atm.

Pore-Size Distribution. The pore size distribution for BPL activated carbon was determined using the experimental data of Russell and LeVan[29] for adsorption of nitrogen on the adsorbent at 77 K and is shown in Figure 3. The log-normal distribution with three modes, given by eq 11, and 35 different pore isotherms like those shown in Figure 2 were used in the

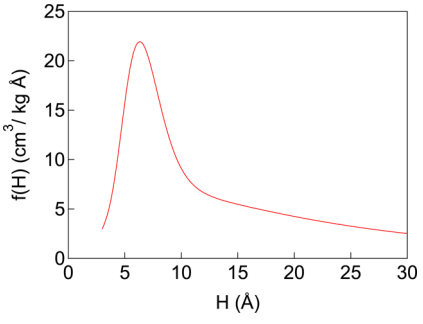

Figure 3. Pore size distribution calculated from nitrogen density profiles using a log-normal distribution with three modes as given by eq 11. Parameters are M = 3, $\alpha_1 = 1.127 \times 10^{-5}$, β_1 = 3.415, γ_1 = 0.3813, α_2 = 46.06, β_2 = 3.026, γ_2 = 0.013 16, α_3 = 843.1, β_3 = 3.426, and γ_3 = −0.009 492.

DOI: 10.1021/jp510515m
J. Phys. Chem. C 2015, 119, 1457−1463

calculations. The distribution has a broad peak near 6 Å and a long tail that decreases as pore width increases.

The pore size distribution is similar in shape to that calculated by Russell and LeVan[29] from their measured isotherm. They used the single pore isotherms calculated from DFT by Seaton et al.,[39] where nitrogen was treated as spherical with a mean-field assumption. The calculated pore size distribution had its main peak at 11 Å. However, our individual pore isotherms show higher capacities than those calculated by Russell and LeVan, which leads to lower peak heights in the pore size distribution to give similar overall amounts of nitrogen adsorbed.

Figure 4 shows the experimental data and the calculated nitrogen isotherm corresponding to the calculated pore size

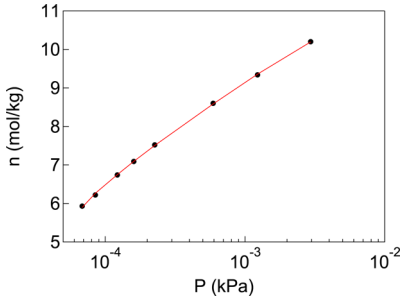

Figure 4. Nitrogen isotherm at 77 K on BPL activated carbon. Solid curve is the calculated isotherm.

distribution. The isotherm describes the data well. We are unable to determine if the theory can replicate the small hump in the isotherm that has been observed in experiments[40] because the hump occurs at pressures higher than those used to determine the pore size distribution.

Prediction of Alkane Isotherms. Alkane isotherms can now be predicted purely from the parameters in Table 1 and the pore size distribution. Excess isotherms for adsorption of *n*-alkanes at 298.15 and 348.15 K were predicted using the adsorption integral equation, eq 10, and 35 calculated pore isotherms for each alkane. The density profiles comprising the single pore isotherms for the *n*-alkanes are not as sharp as those for nitrogen, as a consequence of the much higher adsorption temperatures. As examples, some density profiles and single pore isotherms for *n*-pentane adsorbed in carbon slit pores at 298.15 K are shown in the Supporting Information.

The methane and ethane isotherms on BPL carbon are shown in Figures 5 and 6 and are compared to experimental data of Pigorini.[30,31] The isotherm is predicted well at 298.15 K,

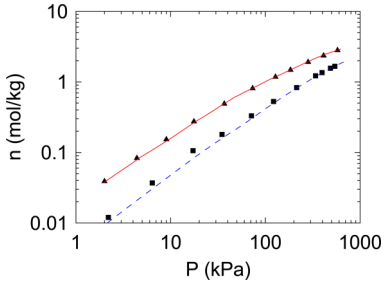

Figure 5. Methane isotherms at 298.15 K (▲) and 348.15 K (■) on BPL activated carbon. Data points are experimental measurements of Pigorini.[30,31] Curves are predicted.

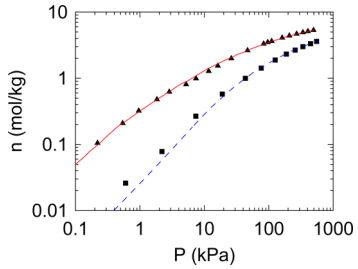

Figure 6. Ethane isotherms at 298.15 K (▲) and 348.15 K (■) on BPL activated carbon. Data points are experimental measurements of Pigorini.[30,31] Curves are predicted.

but data at 348.15 K at low pressures are somewhat underpredicted. Overall, however, the isotherm predictions generally agree well with the experimental data. The predicted isotherms for *n*-butane on BPL carbon are shown in Figure 7.

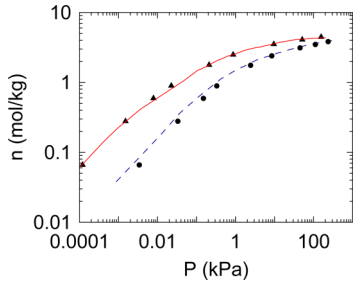

Figure 7. Butane isotherms at 298.15 K (▲) and 348.15 K (■) on BPL activated carbon. Data points are experimental measurements of Pigorini.[30,31] Curves are predicted.

The isotherm predicts the experimental data well at 298.15 K but somewhat overpredicts the measured adsorbed-phase concentrations at 348.15 K. The predicted isotherms for *n*-pentane adsorption on BPL carbon at 298.15 and 348.15 K are shown in Figure 8, where they are compared with the

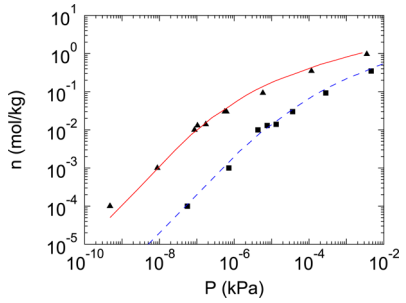

Figure 8. *n*-Pentane isotherms at 298.15 K (▲) and 348.15 K (■) on BPL activated carbon. Data points are experimental measurements of Schindler.[32] Curves are predicted.

experimental data of Schindler et al.,[32] which were measured with a specialized apparatus and extend to ultralow concentrations in the Henry's law region. The experimental isotherms have a slight plateau around 10^{-7} and 10^{-5} kPa (for 298.15 and 348.15 K, respectively) due to overlap from the use of two loading procedures. The predicted isotherms transition smoothly into this linear region and are in good agreement with the experimental data over the entire range for both temperatures. The calculated isotherms of *n*-hexane on BPL

DOI: 10.1021/jp510515m
J. Phys. Chem. C 2015, 119, 1457−1463

carbon, shown in Figure 9, agree well with the experimental data of Pigorini[30,31] at both 298.15 and 348.15 K.

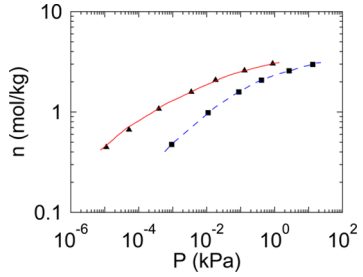

Figure 9. *n*-Hexane isotherms at 298.15 K (▲) and 348.15 K (■) on BPL activated carbon. Data points are experimental measurements of Pigorini.[30,31] Curves are predicted.

The successful prediction of adsorption of the alkanes for the progression of chain lengths and use of a pore size distribution based on nitrogen adsorption at cryogenic temperature show that the theory in the SAFT-FMT-DFT approach is capable of accurately predicting adsorption isotherms for a wide range of molecules at a variety of temperatures using a single set of parameters determined independently for each molecule.

4. CONCLUSIONS

This paper is the first application of the SAFT-FMT-DFT approach to experimental data. The theory has been used to specify interaction parameters of nitrogen, methane, ethane, *n*-butane, *n*-pentane, and *n*-hexane with a planar carbon wall. These were used to determine single pore isotherms for the adsorbates in carbon slit pores. The calculated density profiles for adsorption of nitrogen at 77 K show monolayer transitions, pore filling, and pore condensation. Apparent layering interactions are created in pore widths where large density peaks are closer than 1 σ_{ff} apart in the center of the pore. Pore condensation was observed with the bases of the density peaks narrowing and the heights of the peaks increasing.

A pore size distribution with an assumed log-normal distribution with three modes was determined for BPL activated carbon using experimental data for nitrogen adsorption at 77 K and the single pore isotherms for nitrogen. The pore size distribution was used with *n*-alkane single pore isotherms to predict *n*-alkane isotherms for adsorption on BPL activated carbon at 298.15 and 348.15 K. The predicted isotherms compare well with measured isotherms.

The SAFT−FMT−DFT approach has been shown to be useful for estimating a pore size distribution from experimental data measured at cryogenic temperature and for calculating isotherms for a range of other molecules at much higher temperatures using the pore size distribution. This approach should be useful for predicting the adsorption of many other chain molecules.

■ ASSOCIATED CONTENT

Supporting Information

Figures for fits of fluid−fluid and solid−fluid parameters; contributions of $-CH_3$ and $-CH_2-$ groups to the alkane parameters; density profiles and single pore isotherms for *n*-pentane adsorbed in carbon slit pores at 298.15 K. This material is available free of charge via the Internet at http://pubs.acs.org.

■ AUTHOR INFORMATION

Corresponding Author

*Tel (615) 322-2441; Fax (615) 343-7951; e-mail m.douglas.levan@vanderbilt.edu (M.D.L).

Notes

The authors declare no competing financial interest.

■ ACKNOWLEDGMENTS

Financial support for this research was provided in part by the U.S. Department of Energy (DOE), Office of Basic Energy Sciences, Geoscience Research Program, through Grant ERKCC72 of Oak Ridge National Laboratory, which is managed for DOE by UT Battelle, LLC, under Contract DE-AC05- 00OR22725.

■ REFERENCES

(1) Schindler, B. J.; Mitchell, L. A.; McCabe, C.; Cummings, P. T.; LeVan, M. D. Adsorption of Chain Molecules in Slit-Shaped Pores: Development of a SAFT-FMT-DFT Approach. *J. Phys. Chem. C* **2013**, *117*, 21337−21350.

(2) Lastoskie, C.; Gubbins, K. E.; Quirke, N. Pore Size Distribution Analysis of Microporous Carbons: A Density Functional Theory Approach. *J. Phys. Chem.* **1993**, *97*, 4786−4796.

(3) Lastoskie, C.; Gubbins, K. E.; Quirke, N. Pore Size Heterogeneity and the Carbon Slit Pore: A Denstiy Functional Theory Model. *Langmuir* **1993**, *9*, 2693−2702.

(4) Ryu, Z.; Zheng, J.; Wang, M.; Zhang, B. Characterization of Pore Size Distributions on Carbonaceous Adsorbents by DFT. *Carbon* **1999**, *37*, 1257−1264.

(5) Dombrowski, R. J.; Hyduke, D. R.; Lastoskie, C. M. Pore Size Analysis of Activated Carbons from Argon and Nitrogen Porosimetry Using Density Functional Theory. *Langmuir* **2000**, *16*, 5041−5050.

(6) Ustinov, E. A.; Do, D. D.; Fenelonov, V. B. Pore Size Distribution Analysis of Activated Carbons: Application of Density Functional Theory Using Nongraphitized Carbon Black as a Reference System. *Carbon* **2006**, *44*, 653−663.

(7) Ravikovitch, P. I.; Haller, G. L.; Neimark, A. V. Density Functional Theory Model for Calculating Pore Size Distributions: Pore Structure on Nanoporous Catalysts. *Adv. Colloid Interface Sci.* **1998**, *76−77*, 203−226.

(8) Tanaka, H.; El-Merraoui, M.; Steele, W. A.; Kaneko, K. Methane Adsorption on Single-Walled Carbon Nanotube: A Density Functional Theory Model. *Chem. Phys. Lett.* **2002**, *352*, 334−341.

(9) Carati, A.; Ferraris, G.; Guidotti, M.; Moretti, G.; Psaro, R.; Rizzo, C. Preparation and Characterisation of Mesoporous Silica-Alumina and Silica-Titania with a Narrow Pore Size Distribution. *Catal. Today* **2003**, *4*, 315−323.

(10) Figueroa-Gerstenmaier, S.; Bonet Avalos, J.; Gelb, L. D.; Gubbins, K. E.; Vega, L. F. Pore Size Distribution of Porous Glasses: A Test of the Independent Pore Model. *Langmuir* **2003**, *19*, 8592−8604.

(11) Zhang, S.; Shao, T.; Kose, H. S.; Karanfil, T. Adsorption of Aromatic Compounds by Carbonaceous Adsorbents: A Comparative Study on Granular Activated Carbon, Activated Carbon Fiber, and Carbon Nanotubes. *Environ. Sci. Technol.* **2010**, *44*, 6377−6383.

(12) Hornebecq, V.; Knöfel, C.; Boulet, P.; Kuchta, B.; Llewellyn, P. L. Adsorption of Carbon Dioxide on Mesoporous Zirconia: Microcalorimetric Measurements, Adsorption Isotherm Modeling, and Density Functional Theory Calculations. *J. Phys. Chem. C* **2011**, *115*, 10097−10103.

(13) Gor, G. Y.; Thommes, M.; Cychosz, K. A.; Neimark, A. V. Quenched Solid Density Functional Theory Method for Characterization of Mesoporous Carbons by Nitrogen Adsorption. *Carbon* **2012**, *50*, 1583−1590.

(14) Landers, J.; Gor, G. Y.; Neimark, A. V. Density Functional Theory Methods for Characterization of Porous Materials. *Colloids Surf., A* **2013**, *437*, 3−32.

DOI: 10.1021/jp510515m
J. Phys. Chem. C 2015, 119, 1457−1463

(15) Chapman, W. G.; Gubbins, K. E.; Jackson, G.; Radosz, M. SAFT: Equation-of-State Solution Model for Associating Fluids. *Fluid Phase Equilib.* **1989**, *52*, 31−38.
(16) Wertheim, M. S. Fluids with Highly Directional Attractive Forces. I. Statistical Thermodynamics. *J. Stat. Phys.* **1984**, *35*, 19−34.
(17) Wertheim, M. S. Fluids with Highly Directional Attractive Forces. II. Thermodynamic Perturbation Theory and Integral Equations. *J. Stat. Phys.* **1984**, *35*, 35−47.
(18) Wertheim, M. S. Fluids with Highly Directional Attractive Forces. III. Multiple Attraction Sites. *J. Stat. Phys.* **1986**, *42*, 459−476.
(19) Wertheim, M. S. Fluids with Highly Directional Attractive Forces. IV. Equilibrium Polymerization. *J. Stat. Phys.* **1986**, *42*, 477−492.
(20) McCabe, C.; Galindo, A. SAFT Associating Fluids and Fluid Mixtures. In *Applied Thermodynamics of Fluids*; Goodwin, A. R. H., Sengers, J. V., Peters, C. J., Eds.; Royal Society of Chemistry: London, 2010.
(21) Gil-Villegas, A.; Galindo, A.; Whitehead, P. J.; Mills, S. J.; Jackson, G.; Burgess, A. N. Statistical Associating Fluid Theory for Chain Molecules with Attractive Potentials of Variable Range. *J. Chem. Phys.* **1997**, *106*, 4168−4186.
(22) Rosenfeld, Y. Free-Energy Model for the Inhomogeneous Hard-Sphere Fluid Mixture and Density-Functional Theory of Freezing. *Phys. Rev. Lett.* **1989**, *63*, 980−983.
(23) Rosenfeld, Y.; Schmidt, M.; Lowen, H.; Tarazona, P. Fundamental-Measure Free-Energy Density Functional for Hard Spheres: Dimensional Crossover and Freezing. *Phys. Rev. E* **1997**, *55*, 4245−4263.
(24) Shen, G.; Ji, X.; Lu, X. A Hybrid Perturbed-Chain SAFT Density Functional Theory for Representing Fluid Behavior in Nanopores. *J. Chem. Phys.* **2013**, *138*, 224706.
(25) Shen, G.; Ji, X.; Öberg, S.; Lu, X. A Hybrid Perturbed-Chain SAFT Density Functional Theory for Representing Fluid Behavior in Nanopores: Mixtures. *J. Chem. Phys.* **2013**, *139*, 194705.
(26) Tripathi, S.; Chapman, W. G. Microstructure of Inhomogeneous Polyatomic Mixtures from a Density Functional Formalism for Atomic Mixtures. *J. Chem. Phys.* **2005**, *122*, 094506.
(27) Malheiro, C.; Mendiboure, B.; Plantier, F.; Blas, F. J.; Miqueu, C. Density Functional Theory for the Description of Spherical Non-Associating Monomers in Confined Media Using the SAFT-VR Equation of State and Weighted Density Approximations. *J. Chem. Phys.* **2014**, *140*, 134707.
(28) Steele, W. A. The Physical Interaction of Gases with Crystalline Solids. I. Gas-Solid Energies and Properties of Isolated Adsorbed Atoms. *Surf. Sci.* **1973**, *36*, 317−352.
(29) Russell, B. P.; LeVan, M. D. Pore Size Distribution of BPL Activated Carbon Determined by Different Methods. *Carbon* **1994**, *32*, 845−855.
(30) Walton, K. S.; Pigorini, G.; LeVan, M. D. Simple Group Contribution Theory for Adsorption of Alkanes in Nanoporous Carbons. *Chem. Eng. Sci.* **2004**, *59*, 4423−4430.
(31) Pigorini, G. Periodic Behavior of Pressure Swing Adsorption Cycles and Coadsorption of Light and Heavy n-Alkanes on Activated Carbon. University of Virginia, Charlottesville, VA; Ph.D. Dissertation, 2000.
(32) Schindler, B. J.; Buettner, L. C.; LeVan, M. D. Transition to Henry's Law in Ultra-Low Concentration Adsorption Equilibrium for n-Pentane on BPL Activated Carbon. *Carbon* **2008**, *46*, 1285−1293.
(33) Hansen-Goos, H.; Roth, R. Density Functional Theory for Hard Sphere Mixtures: the White Bear Version Mark II. *J. Phys.: Condens. Matter* **2006**, *18*, 8413−8425.
(34) Yu, Y. X.; Wu, J. Z. Density Functional Theory for Inhomogeneous Mixtures of Polymeric Fluids. *J. Chem. Phys.* **2002**, *117*, 2368−2376.
(35) Kirkpatrick, S.; C.D. Gelatt, C. D.; Vecchi, M. P. Optimization by Simulated Annealing. *Science* **1983**, *220* (4598), 671−680.
(36) Dolan, W. B.; Cummings, P. T.; LeVan, M. D. Process Optimization via Simulated Annealing Application to Network Design. *AIChE J.* **1989**, *35*, 725−736.
(37) Kruk, M.; Li, Z.; Jaroniec, M. Nitrogen Adsorption Study of Surface Properties of Graphitized Carbon Blacks. *Langmuir* **1999**, *15*, 1435−1441.
(38) Avgul, N. N.; Kiselev, A. V. Physical Adsorption of Gases and Vapors on Graphitized Carbon Blacks. In *Chemistry and Physics of Carbon*; Walker, P., Ed.; M. Dekker: New York, 1970; Vol. *6*.
(39) Seaton, N. A.; Walton, J. P. R. B.; Quirke, N. A New Analysis Method for the Determination of the Pore Size Distribution of Porous Carbons from Nitrogen Adsorption Measurements. *Carbon* **1989**, *27*, 853−861.
(40) Rouquerol, J.; Partyka, S.; Rouquerol, F. Calorimetric Evidence for a Bidimensional Phase Change in the Monolayer of Nitrogen or Argon Adsorbed on Graphite at 77 K. *J. Chem. Soc., Faraday Trans. 1* **1977**, *73*, 306−314.

DOI: 10.1021/jp510515m
J. Phys. Chem. C 2015, 119, 1457−1463